

A STOCHASTIC PERTURBATION APPROACH TO NONLINEAR BIFURCATING PROBLEMS

ISABELLA CARLA GONNELLA¹, MOAAD KHAMLICH¹, FEDERICO PICHI^{1,2}, GIANLUIGI ROZZA¹

ABSTRACT. Incorporating probabilistic terms in mathematical models is crucial for capturing and quantifying uncertainties of real-world systems. However, stochastic models typically require large computational resources to produce meaningful statistics. For such reason, the development of reduction techniques becomes essential for enabling efficient and scalable simulations of complex scenarios while quantifying the underlying uncertainties. In this work, we study the accuracy of Polynomial Chaos (PC) surrogate expansion of the probability space on a bifurcating phenomena in fluid dynamics, namely the Coandă effect. In particular, we propose a novel non-deterministic approach to generic bifurcation problems, where the stochastic setting gives a different perspective on the non-uniqueness of the solution, also avoiding expensive simulations for many instances of the parameter. Thus, starting from the formulation of the Spectral Stochastic Finite Element Method (SSFEM), we extend the methodology to deal with solutions of a bifurcating problem, by working with a perturbed version of the deterministic model. We discuss the link between the deterministic and the stochastic bifurcation diagram, highlighting the surprising capability of PC polynomials coefficients of giving insights on the deterministic solution manifold.

Keywords: *Bifurcation Problems, Coandă Effect, Polynomial Chaos Expansion, Spectral Stochastic Finite Element, Model Order Reduction, Uncertainty Quantification.*

Code availability: <https://github.com/ICGonnella/SSFEM-Coanda-Effect.git>

1. INTRODUCTION

Nonlinear parametric partial differential equations (PDEs) play a fundamental role in accurately modeling several physics problems, but their solutions may exhibit a non-trivial dependence on the system parameters. This is indeed the case of bifurcating phenomena [40], where the nonlinear terms in the equations give rise to a non-differentiable evolution of the solution manifold, and thus to the non-uniqueness of the solution with respect to the parameters. More specifically, the problem admits multiple co-existing states for the same value of a parameter μ (e.g. controlling the physical properties of the model), and an in-depth numerical investigation is needed to deal with such ill-posedness in order to fully describe the system in the simulations. Studying a model's bifurcating behavior means evaluating the curve individuated in the state space by the solutions obtained solving the equations for different values of the parameters. An intuitive way of describing the bifurcation is to represent it via the *bifurcation diagram*, which consists in tracking a specific scalar quantity of interest, characterizing the different *branches* w.r.t. the corresponding parameter value, possibly including information regarding their stability properties.

The complexity of the topic, coupled with its broad range of potential applications, has stimulated the development of numerical methods to investigate such problems and enhance their exploitation. In particular, *continuation methods* consist in the use of deterministic numerical solvers in an iterative pipeline, progressively exploring the parametric space [1]. The idea behind this approach is to accurately “continue” an already known solution branch in the yet unexplored regions, following its evolution. Nevertheless, the local nature of continuation methods creates a problem when interested in the behavior of the system far from the bifurcation point. Indeed, continuing all the branches for many parameter values easily becomes computationally unbearable, especially when employing

¹ MATHLAB, MATHEMATICS AREA, SISSA, VIA BONOMEA 265, I-34136 TRIESTE, ITALY

² MCSS, ÉCOLE POLYTECHNIQUE FÉDÉRALE DE LAUSANNE, 1015 LAUSANNE, SWITZERLAND

full-order methodologies such as the Finite Element Method (FEM) [38], or when forced to take only small exploration steps.

Several efforts have been dedicated to reduce the computational complexity associated with the reconstruction of the bifurcation diagram and the detection of the bifurcation points, e.g. via the development of ad-hoc surrogate models [31]. Despite this, a complete and computationally affordable investigation of bifurcation problems is still far from being reached.

When dealing with such bifurcation problems in engineering contexts, to properly model the real-life physical behavior it is fundamental to keep into consideration the relevance of the intrinsic uncertainty in the parameters measurements, which could lead to significant evaluation errors in case of non-uniqueness. Indeed, in such cases, the solution of deterministic numerical solvers strictly depends on the initial guess passed to the solver, and different initialization possibly correspond to qualitatively different solutions which belong to different branches even with a little variation of the parameters value. According to this, stochastic approaches incorporating uncertainty quantification techniques have in general been proposed in the standard setting in [18, 51, 14], leading to the formulation of the bifurcation problem in stochastic PDEs, defined as a “noisy version” of the deterministic one [5]. Indeed, by considering the parameters characterizing the physics of the system as a source of uncertainty (boundary conditions, physical parameters, and geometry), the stochastic PDEs inherently incorporate the characteristic randomness typical of real-world scenarios. The importance of such research line is confirmed by the recent work [27], where the authors investigate the statistical properties of the random bifurcation points for the Allen–Cahn equation.

The objective of the the present work is to propose a stochastic-perturbation framework for a detailed and computationally affordable analysis of bifurcating phenomena, aiming at enabling the characterization of the solution branches of the deterministic problem without any prior knowledge of the solution manifold. The idea is to capture the dynamics of the deterministic bifurcation diagram under small perturbations of the parameters around the value of interest, thus releasing the need of performing a continuation approach on every branch to infer their topology. Indeed, as underlined before, while existing numerical methodologies provide valuable tools for a strictly local analysis around the bifurcation point, there persist challenges in efficiently reconstructing solution branches across extensive parametric ranges.

Specifically, we are interested in the capability of the Polynomial Chaos (PC) [47, 55] surrogate model to obtain accurate information on the branches evolution in the parametric space. PC has indeed become increasingly prominent in stochastic computation to properly model the stochastic parameters in PDEs. Precisely, treating pivotal parameters as random variables, PC yields probability density functions (PDFs) linked with the quantities of interest of the system. As such, both the propagation of stochastic terms through the equations and the peculiar properties of the PC expansion furnish insights into the properties of the solution, facilitating its investigation from the statistical standpoint.

To obtain a PC formulation of any stochastic PDEs, we considered the Spectral Stochastic Finite Element Method (SSFEM) pipeline [46], which extends the well known FEM projection approach to the probabilistic setting under investigation. Namely, we first model the parameter of the system as a known stochastic processes that can be expanded over the eigenfunctions of the covariance matrix, i.e. the so-called Karhunen-Loève (K-L) expansion. Then, we write the unknowns of the system in the PC form, exploiting the previously computed eigenfunctions as basic random variables. Solving the stochastic PDE now means finding the PC coefficients for the solution, typically via a generic nonlinear solver. Finally, once obtained such representation, a statistical analysis on the solution can be easily performed thanks to the orthogonal properties of the PC polynomials, which enable the computation of the statistical moments through proper combinations of the coefficients themselves. A schematic overview of the developed pipeline is illustrated in Figure 1.

In this work, we study the results of SSFEM applied to a specific and well-known bifurcating phenomenon in computational fluid dynamics: the Coandă effect [37]. We consider the viscosity of the fluid as a random variable, indeed, given its role in the bifurcation, this step is fundamental to investigate how its mean and variance influence the velocity field solution.

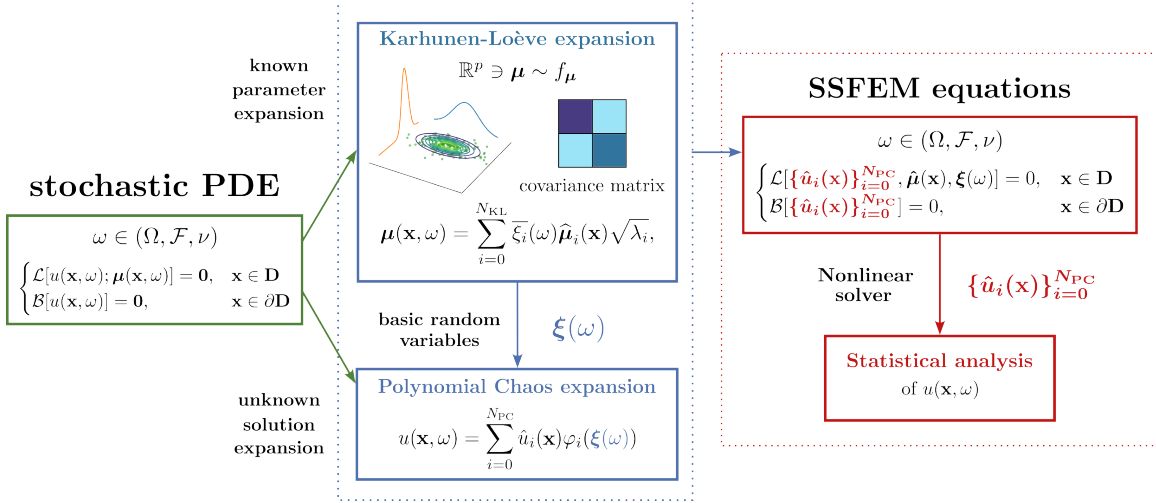


FIGURE 1. Statistical analysis of bifurcations via the stochastic-perturbation approach.

We focus our analysis on the shape of the polynomial solutions in the probability space, and on the statistical moments obtained through the SSFEM approach. Moreover, we discuss the connection between the polynomial expansion of the solution probability distribution and the deterministic bifurcating branches of the non-perturbed system, which, up to our knowledge, has not been pointed out in literature yet and could open interesting scenarios.

We firstly introduce in Section 3 the two expansions used in the SSFEM setting, through which we are able to represent a generic second-order stochastic process in a finite-dimensional space: the K-L and the PC expansions. Moreover, their inclusion in the context of stochastic PDEs is argued, together with a comparison between non-intrusive sample-based and intrusive methods, discussing the problem of retrieving the solution expansion coefficients in the bifurcating setting. Successively, we proceed with the description of the SSFEM intrusive approach in Section 4, presenting its application to the specific context of the Navier-Stokes equations for the Coandă effect in Section 5. Successively, in Section 6 we show the numerical results, underlying the relation discovered between the PC stochastic surrogate model of the solution and its deterministic bifurcation diagram. In particular, the correlation between the PC coefficients and the computational mesh is argued, together with their evolution with the change of probability distribution assigned to the viscosity parameter. Finally, we conclude showing a reproduction of the related deterministic bifurcation diagram, which we obtain only relying on the information collected through the stochastic perturbation approach.

2. RELATED WORKS

The study of bifurcating phenomena in nonlinear PDEs has been a subject of extensive research due to its relevance in various physical and engineering domains [2]. Traditional numerical methods [12], including the Finite Element Method [16] and Spectral Element Method [35], have been widely employed to explore the coexisting solution branches and the critical regime in a neighborhood of the bifurcation points. Indeed, several numerical methodologies are needed to effectively explore and control the global behavior of the system, such as continuation techniques [1] and deflation methods [20]. These tools are respectively designed to reconstruct a specific solution branch, and discover new admissible ones as parameters vary. Moreover, one could also be interested in adopting control strategies on a bifurcation problem, in order to control its behaviour in the parameters space by acting on physics or geometry [34, 9].

When dealing with complex problems, the computational effort associated with all these tasks for a complete exploration of the model could be unbearable. Recent works focused on developing reduced-order models (ROMs) [24, 7] to enable many-query simulations, and thus recovering efficiently the full bifurcating pattern. These approaches can be divided in two categories: the ones exploiting standard projection-based techniques [31, 36, 26, 35], and the data-driven ones, often based on machine-learning strategies [11, 32, 33, 17].

All the above works treat the bifurcation problem in absence of randomness. Indeed, the deterministic assumption simplifies the analysis of the system’s behavior, not requiring the additional computational burden typical of stochastic settings, but it is often not physically realistic. For this reason, the presence of stochasticity in the models cannot be disregarded for a comprehensive analysis of the topic, as bifurcating phenomena depend on various uncertainties due to input variability, parameter uncertainty, and numerical discretization [42].

Towards a more realistic study of the problem, the concept of bifurcation has been expanded in the stochastic setting with the analysis of additive and multiplicative noise effects on the models, thus characterizing various types of *stochastic bifurcations* [5]. Indeed, while in the deterministic case the bifurcation corresponds to a qualitative change in the dynamics of the system as a response to a small variation of the parameters, in the stochastic case it can be observed as a sudden change in some invariant measure of the system’s solution as a result of some imposed additive or multiplicative perturbation. Such changes can involve variations in the largest Lyapunov exponent (*dynamical bifurcations*), as well as changes in the shape of the solution probability density function (*phenomenological bifurcations*) [4].

Early investigations explored the dynamic response, stability, and bifurcating behavior of nonlinear dynamical systems under stochastic excitation. In [45], the author studied the impact of small stochastic perturbations on systems exhibiting codimension-one and -two bifurcations. The work exploited methods of stochastic averaging and stochastic normal forms to analyze the asymptotic behavior of nonlinear dynamical systems in the presence of noise.

Furthermore, various works have been conducted for specific systems of equations, such as the stochastic reaction-diffusion equation perturbed by an infinite-dimensional Wiener process in [8], and the stochastic regime-switching predator–prey system in [29]. Moreover, investigating the interplay between deterministic and stochastic bifurcations, the authors in [30] propose a method to derive probabilistic bifurcation diagrams for stochastic nonlinear dynamical systems using the Fokker-Planck equation.

Going in the direction of identifying the stochastic perturbation applied to the system with the randomness associated to its parameters, in [50], the authors explore a stochastic approach to the known deterministic bifurcations in Rayleigh–Bénard convection within a two-dimensional cavity. The study investigates the onset of instability, and the existence of multiple stable states under specific ranges of Rayleigh number. Indeed, through stochastic simulations conducted around a point of deterministic bifurcation, the authors reveal the influence of also random initial flow states on convection patterns. The importance of stochastic aspects has been highlighted via Monte Carlo simulations in [39], investigating the probabilities of the solution branches through a stochastic sampling of the parameterized initial conditions. Moreover, they introduce a comparison between the accuracy of statistical moments computation of Monte Carlo sampling and the PC expansion of the solution, confirming the high reliability and computational convenience of the latter.

3. STOCHASTIC MODELING IN PDES: STOCHASTIC EXPANSIONS

Given an established deterministic model for a physical system, we want to define a convenient setup for its stochastic counterpart, to study the effect of uncertainty in the input parameters on the system itself.

As illustrated in Figure 1, the starting point of such analysis is the characterization of the random input parameters $\boldsymbol{\mu}(\mathbf{x}, \omega) : \mathcal{D} \times \Omega \rightarrow \mathbb{R}^p$ for a stochastic PDE of the form:

$$(1) \quad \begin{cases} \mathcal{L}[u(\mathbf{x}, \omega); \boldsymbol{\mu}(\mathbf{x}, \omega)] = 0 & \mathbf{x} \in \mathcal{D}, \quad \omega \in \Omega, \\ \mathcal{B}[u(\mathbf{x}, \omega)] = 0 & \mathbf{x} \in \partial\mathcal{D}, \quad \omega \in \Omega, \end{cases}$$

where \mathcal{L} and \mathcal{B} incorporate respectively the physics and the boundary constraints, $u(\mathbf{x}, \omega) : \mathcal{D} \times \Omega \rightarrow \mathbb{R}$ is the unknown solution of the system, $\mathcal{D} \subset \mathbb{R}^n$ the spatial domain, and $(\Omega, \mathcal{F}, \nu)$ a probability space, where (Ω, \mathcal{F}) is a measurable space with \mathcal{F} a σ -algebra defined on Ω , and ν a probability measure on it. We recall that a generic real stochastic process is defined as a family $\boldsymbol{\alpha}(\mathbf{x}, \omega) = \{\boldsymbol{\alpha}(\mathbf{x}, \cdot)\}_{\mathbf{x} \in \mathcal{D}}$ of random variables, which are in turn measurable functions of the type $\boldsymbol{\alpha}(\mathbf{x}, \cdot) : (\Omega, \mathcal{F}, \nu) \rightarrow (\mathbb{R}^d, \mathcal{B})$ for a generic $d \leq \infty$.

By considering the solution as a generic stochastic process $\boldsymbol{\alpha}(\mathbf{x}, \omega)$, to enable numerical computations we need to reduce the infinite-dimensional probability space to a finite-dimensional one. This is accomplished by exploiting a decomposition of the stochastic process via a finite set of random variables.

We are interested in obtaining meaningful expansions of the real stochastic processes $\boldsymbol{\alpha}(\mathbf{x}, \omega)$ having finite second-order moment, thus belonging to the space: $\mathbb{L}_2(\Omega, \mathcal{F}, \nu; \mathbb{R}^d) := \{\boldsymbol{\alpha}(\mathbf{x}, \omega) : \mathcal{D} \times \Omega \rightarrow \mathbb{R}^d \text{ s.t. } \mathbb{E}[\boldsymbol{\alpha}^2(\mathbf{x}, \cdot)] = \int_{\Omega} \boldsymbol{\alpha}(\mathbf{x}, \omega)^2 d\nu(\omega) < \infty\}$. Now, we introduce two well-known methodologies: the Karhunen-Loève and the Polynomial Chaos expansions, which constitute the basis for the generalization of FEM in the probabilistic context, towards the definition of the Spectral Stochastic Finite Element Method.

3.1. Karhunen-Loève expansion. The Karhunen-Loève (K-L) expansion [52, 3] operates similarly to the Fourier expansion but it applies to the space of stochastic processes with finite second-order moment $\mathbb{L}_2(\Omega, \mathcal{F}, \nu; \mathbb{R}^d)$. The main idea of the method is to first find the orthonormal eigenfunctions $\boldsymbol{\pi}_i(\mathbf{x})$ of the Hilbert-Schmidt integral operator \mathcal{H}_K defined as:

$$(2) \quad \mathcal{H}_K[\boldsymbol{\pi}_i(\mathbf{x})](\mathbf{x}) = \int_{\mathcal{D}} K_{\boldsymbol{\alpha}}(\mathbf{x}, \mathbf{y}) \boldsymbol{\pi}_i(\mathbf{y}) d\mathbf{y} = \lambda_i \boldsymbol{\pi}_i(\mathbf{x}),$$

whose kernel $K_{\boldsymbol{\alpha}}(\mathbf{x}, \mathbf{y})$ is the covariance function of the process $\boldsymbol{\alpha}(\mathbf{x}, \omega) \in \mathbb{L}_2(\Omega, \mathcal{F}, \nu; \mathbb{R}^d)$, and λ_i are the eigenvalues associated with $\boldsymbol{\pi}_i(\mathbf{x})$. Subsequently, the process is projected onto such orthonormal basis, obtaining the random variables:

$$(3) \quad \xi_i(\omega) = \int_{\mathcal{D}} \boldsymbol{\alpha}(\mathbf{x}, \omega) \boldsymbol{\pi}_i(\mathbf{x}) d\mathbf{x} \quad \text{s.t.} \quad \mathbb{E}[\xi_i] = 0, \text{ and } \mathbb{E}[\xi_i \xi_j] = \lambda_i \delta_{i,j},$$

where the conditions on their mean and variance are easily obtained substituting the $\boldsymbol{\pi}_i(\mathbf{x})$ functions with their definition in Equation (2). Namely, they are orthogonal in the space $\mathbb{L}_2(\Omega, \mathcal{F}, \nu; \mathbb{R}^d)$, and thus uncorrelated. The K-L expansion can then be expressed as:

$$(4) \quad \boldsymbol{\alpha}(\mathbf{x}, \omega) = \bar{\boldsymbol{\alpha}}(\mathbf{x}) + \sum_{i=1}^{\infty} \frac{\xi_i(\omega)}{\sqrt{\lambda_i}} \boldsymbol{\pi}_i(\mathbf{x}) \sqrt{\lambda_i} = \sum_{i=0}^{\infty} \bar{\xi}_i(\omega) \boldsymbol{\pi}_i(\mathbf{x}) \sqrt{\lambda_i},$$

where the first two equivalence follow directly from introducing the normalized random variables $\bar{\xi}_i(\omega)$ such that $\mathbb{E}[\bar{\xi}_i] = 0$ and $\mathbb{E}[\bar{\xi}_i \bar{\xi}_j] = \delta_{i,j}$, and assuming without loss of generality that $\bar{\xi}_0(\omega) \sim \mathcal{N}(1, 0)$, $\boldsymbol{\pi}_0(\mathbf{x}) = \bar{\boldsymbol{\alpha}}(\mathbf{x})$, and $\lambda_0 = 1$.

The convergence properties of this expansion clearly strictly depend on the nature of the stochastic process covariance function, namely on the decay of its eigenvalues. For a further discussion on the topic we refer to [25]. In general, it is to be noted that the K-L expansion is particularly useful to model the parameters of a generic stochastic PDE (1), since their covariance function is known and all the computation comes down to its spectral study.

3.2. Polynomial Chaos expansion. The PC expansion decomposes a general stochastic process $\alpha(\mathbf{x}, \omega) \in \mathbb{L}_2(\Omega, \mathcal{F}, \nu; \mathbb{R}^d)$ thanks to the Cameron-Martin theorem [13], which establishes the existence of a sequence of closed, pairwise orthogonal linear subspaces of $\mathbb{L}_2(\Omega, \mathcal{F}, \nu; \mathbb{R}^d)$, spanned by polynomial bases. In particular, the PC expansion expresses the process $\alpha(\mathbf{x}, \omega)$ as the infinite sum:

$$(5) \quad \alpha(\mathbf{x}, \omega) = \sum_{i=0}^{\infty} \hat{\alpha}_i(\mathbf{x}) \psi_i(\{\zeta_j(\omega)\}_{j=1}^{N_{RV}}), \quad \text{with} \quad \int_{\mathbb{R}^d} \psi_i(\zeta) \psi_j(\zeta) d\nu_{\zeta} = \|\psi_i\|^2 \delta_{i,j},$$

where $\hat{\alpha}_i(\mathbf{x})$ are the expansion coefficients associated with the stochastic polynomial basis $\psi_i(\{\zeta_j(\omega)\}_{j=1}^{N_{RV}}) : (\Omega, \mathcal{F}, \nu) \rightarrow \mathbb{R}$, which are orthogonal with respect to the Gaussian measure ν_{ζ} and depending on N_{RV} independent standard normal random variables $\zeta_j(\omega)$. We have indicated the set of random variables, called also *seeds* or *basic random variables*, as $\zeta = \{\zeta_j(\omega)\}_{j=1}^{N_{RV}}$. For a Gaussian measure ν_{ζ} , the orthogonal basis corresponds to the set of Hermite polynomials [21]. For computational purposes, the infinite sum in (5) is in practice truncated to a finite number of terms N_{PC} . It is often useful to relate such number to the desired maximum degree M of the polynomials, and the number of variables N_{RV} from which they depend as $1 + N_{PC} = \frac{(M+N_{RV})!}{M!N_{RV}!}$. A generalization of the PC expansion has been presented in [54] with the *generalized Polynomial Chaos* (gPC), in which the expansion is obtained using different classes of polynomials, known as Wiener-Askey polynomials [19], depending on the measure associated to the basic random variables ν_{ζ} , as shown in Table 1.

Type	Basic random variables	Wiener-Askey polynomials	Support
Continuous	Gaussian	Hermite	$(-\infty, \infty)$
	Gamma	Laguerre	$[0, \infty)$
	Beta	Jacobi	$[a, b]$
	Uniform	Legendre	$[a, b]$
Discrete	Poisson	Charlier	$\{0, 1, 2, \dots\}$
	Binomial	Krautchouk	$\{0, 1, 2, \dots, N\}$
	Negative Binomial	Meixner	$\{0, 1, 2, \dots\}$

TABLE 1. Some of the correspondences between basic random variables, the Wiener-Askey orthogonal polynomials for gPC expansion, and their support.

3.3. Intrusive and non-intrusive approaches. In the former sections, we have seen that modeling the stochastic components of the system as random variables and stochastic processes allows us to express them as series expansions. However, a crucial task in this context consists in the determination of the coefficients for such representations when the covariance function is unknown. Indeed, once found their representations, such expansions could also be used to infer relevant information, such as statistical moments. In order to obtain such coefficients knowing the relative bases, one can exploit *intrusive* or *non-intrusive* approaches. While the former class of methodologies requires some knowledge about the original system (e.g. the weak form of the problem for FEM), approaches belonging to the latter class typically treat the solver as a black-box model, from which samples of the solution can be extracted and exploited to retrieve the coefficients (for instance by interpolation).

In general, when well-established deterministic codes exist, sample-based non-intrusive stochastic simulations of the system can be performed, computing the solution for different parameters values [6]. Such methods include Monte Carlo simulation [39], orthogonal spectral projection [53], and stochastic collocation [6]. Monte Carlo simulation gathers a set of solutions by varying input parameters and then deduces statistical properties from the collected data. On the other hand, orthogonal spectral projection aims at determining solution expansion coefficients through numerical integration of its projection integral, while stochastic collocation achieves this via interpolation of sampled deterministic solutions (we refer the reader to [48]).



FIGURE 2. Synthetic workflow diagram showing the process of computing the corresponding PDF of $u(\mathbf{x}, \omega)$ by solving Equation (6) using SSFEM.

In the particular context of bifurcating problems, sample-based approaches may not be suitable. Indeed, deterministic numerical solvers provide results strictly dependent on the given initial guess, often guiding the final solution to a specific branch among all possible ones. Because of this limitation, obtaining reliable statistical information on the solution using some samples of it could be a quite complex and biased task. Thus, such scenarios need the development of intrusive approaches which are independent on the availability of solution samples, in order to retrieve the unknown coefficients of the PC expansion of the solution without relying on the presence of a comprehensive set of data fully descriptive of the solution manifold, as this is in general quite unrealistic.

4. SPECTRAL STOCHASTIC FINITE ELEMENT METHOD

In this section, we recall the general framework of a stochastic PDE presented in Equation (1), and describe the SSFEM pipeline exploiting the two stochastic expansions introduced previously.

Let $\mathcal{D} \subset \mathbb{R}^n$ ($n = 2, 3$) represent a bounded domain, and $(\Omega, \mathcal{F}, \nu)$ denote a probability space. We consider the following general abstract problem:

$$(6) \quad (\mathbf{D}(\mathbf{x}) + \mathbf{S}(\mathbf{x}, \boldsymbol{\mu}(\mathbf{x}, \omega)))u(\mathbf{x}, \omega) = \mathbf{f}(\mathbf{x}) \quad \text{for } \mathbf{x} \in \mathcal{D}, \omega \in \Omega$$

where $u(\mathbf{x}, \omega) : \mathcal{D} \times \Omega \rightarrow \mathbb{R}$ is the unknown function, and $\boldsymbol{\mu}(\mathbf{x}, \omega) : \mathcal{D} \times \Omega \rightarrow \mathbb{R}^p$ represents the p -dimensional stochastic process characterizing the system's parameters. The deterministic operator \mathbf{D} and its stochastic counterpart \mathbf{S} act on $u(\mathbf{x}, \omega)$ returning an object that belongs to \mathbb{R}^{out} , while $\mathbf{f}(\mathbf{x}) : \mathcal{D} \rightarrow \mathbb{R}^{out}$ represents the source term¹. With stochastic and deterministic operators, we intend operators which respectively depend or not from the stochastic variables we inserted in the system, namely $\boldsymbol{\mu}$.

The general workflow we are interested in, reported in a synthetic version in Figure 2, starts with an arbitrary and known covariance function assigned to $\boldsymbol{\mu}$, which is taken to be a stochastic process with finite second-order moments. The final goal is the computation of the corresponding probability density function (PDF) for u through Equation (6), and the analysis of meaningful statistics. We adopted the SSFEM, as it provides a natural extension of FEM enhanced with the notion of stochastic process expansions through an orthogonal decomposition of the space $\mathbb{L}_2(\Omega, \mathcal{F}, \nu; \mathbb{R})$.

Therefore, the stochastic parameters are expanded using the K-L decomposition presented in Section 3.1. Considering the stochastic process $\boldsymbol{\mu}$ with a known covariance function $K_{\boldsymbol{\mu}}(\mathbf{x}, \mathbf{y})$, the decomposition performs a separation of stochastic and deterministic variables:

$$(7) \quad \boldsymbol{\mu}(\mathbf{x}, \omega) = \sum_{i=0}^{N_{KL}} \bar{\xi}_i(\omega) \hat{\boldsymbol{\mu}}_i(\mathbf{x}) \sqrt{\lambda_i},$$

where we denoted by $\hat{\boldsymbol{\mu}}_i(\mathbf{x})$ the eigenfunctions of $K_{\boldsymbol{\mu}}(\mathbf{x}, \mathbf{y})$.

It is important to remark that a straightforward K-L expansion of the solution u is not feasible since its covariance function is not known a-priori. Therefore, the representation of u is achieved via the gPC expansion as a truncated series comprising of the first N_{PC} terms:

$$(8) \quad u(\mathbf{x}, \omega) = \sum_{i=0}^{N_{PC}} \hat{u}_i(\mathbf{x}) \psi_i(\{\bar{\xi}_l(\omega)\}_{l=1}^{N_{KL}}),$$

¹In the following, we will omit the full notation with the dependence on (\mathbf{x}, ω) for u , $\boldsymbol{\mu}$ and \mathbf{f} .

where we used the uncorrelated normalized random variables² $\boldsymbol{\xi}(\omega) := \{\bar{\xi}_j(\omega)\}_{j=1}^{N_{\text{KL}}}$, resulting from the K-L expansion of the parameters, as the $\{\zeta_j(\omega)\}_{j=1}^{N_{\text{RV}}}$ appearing in Equation (5).

For the sake of simplicity, let us consider the case where $p = 1$ and the stochastic operator \mathbf{S} in Equation (6) can be decomposed as $\mathbf{S}(\mu, \mathbf{x}) = \mu \mathbf{S}(\mathbf{x})$. By inserting the formulation of gPC and K-L expansions, respectively for u and μ , into Equation (6), we can rewrite the problem as follows:

$$(9) \quad \left(\mathbf{D}(\mathbf{x}) + \sum_{i=0}^{N_{\text{KL}}} \bar{\xi}_i(\omega) \hat{\mu}_i(\mathbf{x}) \sqrt{\lambda_i} \mathbf{S}(\mathbf{x}) \right) \left[\sum_{j=0}^{N_{\text{PC}}} \hat{u}_j(\mathbf{x}) \psi_j(\boldsymbol{\xi}(\omega)) \right] = \mathbf{f}(\mathbf{x}).$$

Having tackled the stochastic nature of the problem, we can now exploit standard FEM to numerically approximate the formulation obtained in Equation (9). This involves performing a Galerkin projection on the subspace $\mathcal{D}_h \subset \mathcal{D}$ spanned by a set of deterministic basis functions $\{\phi_k(\mathbf{x})\}_{k=1}^{N_{\text{D}}}$. Indeed, we can expand each gPC coefficient with respect to the FEM basis as:

$$(10) \quad \hat{u}_j(\mathbf{x}) = \sum_{k=1}^{N_{\text{D}}} \hat{u}_{k,j} \phi_k(\mathbf{x}), \quad \forall j \in \{0, \dots, N_{\text{PC}}\}.$$

Substituting the former expansion into Equation (9), we obtain the formulation:

$$(11) \quad \left(\mathbf{D}(\mathbf{x}) + \sum_{i=0}^{N_{\text{KL}}} \bar{\xi}_i(\omega) \hat{\mu}_i(\mathbf{x}) \sqrt{\lambda_i} \mathbf{S}(\mathbf{x}) \right) \left[\sum_{j=0}^{N_{\text{PC}}} \sum_{k=1}^{N_{\text{D}}} \hat{u}_{k,j} \phi_k(\mathbf{x}) \psi_j(\boldsymbol{\xi}(\omega)) \right] = \mathbf{f}(\mathbf{x}),$$

that has to be solved for the unknown $\hat{\mathbf{U}} = \{\hat{u}_{k,j}\}_{k=1}^{N_{\text{D}}} \}_{j=0}^{N_{\text{PC}}} \in \mathbb{R}^{N_{\text{D}} \times (N_{\text{PC}}+1)}$. Then, in order to construct an algebraic system of equations for $\hat{\mathbf{U}}$, one imposes the orthogonality of the residual in Equation (11) with respect to the deterministic and stochastic test functions, respectively $\{\phi_n(\mathbf{x})\}_{n=1}^{N_{\text{KL}}}$ and $\{\psi_m(\boldsymbol{\xi})\}_{m=0}^{N_{\text{PC}}}$. The discrete counterpart of the stochastic PDE now reads as the following system of equations $\forall n \in \{1, \dots, N_{\text{D}}\}$, and $\forall m \in \{0, \dots, N_{\text{PC}}\}$:

$$(12) \quad \sum_{j=0}^{N_{\text{PC}}} \sum_{k=1}^{N_{\text{D}}} C_{j,m} \hat{u}_{k,j} A_{k,n} + \sum_{i=0}^{N_{\text{KL}}} \sum_{j=0}^{N_{\text{PC}}} \sum_{k=1}^{N_{\text{D}}} E_{i,j,m} \hat{u}_{k,j} B_{i,k,n} = F_n,$$

having introduced the following notation for the coefficients of the tensors to be assembled:

$$A_{k,n} = \int_{\mathcal{D}} \mathbf{D}(\mathbf{x}) [\phi_k(\mathbf{x})] \phi_n(\mathbf{x}) d\mathbf{x}, \quad B_{i,k,n} = \int_{\mathcal{D}} \hat{\mu}_i(\mathbf{x}) \mathbf{S}(\mathbf{x}) [\phi_k(\mathbf{x})] \phi_n(\mathbf{x}) d\mathbf{x},$$

$$F_n = \int_{\mathcal{D}} \mathbf{f}(\mathbf{x}) \phi_n(\mathbf{x}) d\mathbf{x}, \quad C_{j,m} = \int_{\mathbb{R}^d} \psi_j(\boldsymbol{\xi}) \psi_m(\boldsymbol{\xi}) d\nu_{\boldsymbol{\xi}}, \quad E_{i,j,m} = \int_{\mathbb{R}^d} \bar{\xi}_i \sqrt{\lambda_i} \psi_j(\boldsymbol{\xi}) \psi_m(\boldsymbol{\xi}) d\nu_{\boldsymbol{\xi}}.$$

Therefore, the system can now be solved in function of the unknown $\hat{\mathbf{U}}$ by means of a nonlinear solver, assuming a generic nonlinear nature of the two operators \mathbf{D} and \mathbf{S} . As it will be underlined in the results section, the choice of the solver represents a crucial step for the methodology. Indeed, when interested in simulations involving dense grids (i.e. high N_{D}), and high polynomial degrees (i.e. high N_{PC}), the convergence rate of the solver might be compromised by the number of the degrees of freedom of $\hat{\mathbf{U}}$. In such cases, it is convenient to perform the computations in parallel, splitting the grid between multiple processors and performing separately the residual and update step computation needed by the iterative solver.

4.1. Statistical moments computation. A significant advantage of the gPC representation is that, having obtained the solution coefficients $\hat{\mathbf{U}}$ from Equation (12), it enables an easy computation of the first and second-order moments of the solution. Indeed, leveraging the orthogonality property

²The index for KL random variables starts from 1 due to the assumptions in Section 3.1.

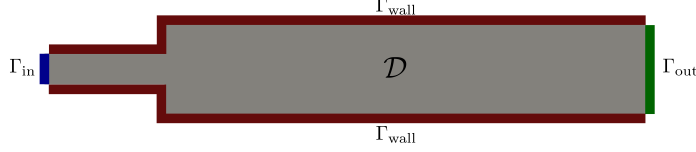


FIGURE 3. Computational domain representing the 2D sudden-expansion channel.

of the polynomials $\{\psi_i\}_{i=1}^{N_{PC}}$ and recognizing that, since the polynomial of degree zero is constant, the following conditions hold $\forall i \in \{0, \dots, N_{PC}\}$:

$$(13) \quad \mathbb{E}[\psi_i(\boldsymbol{\xi})] = \mathbb{E}[\psi_i(\boldsymbol{\xi})\psi_0(\boldsymbol{\xi})] = \delta_{i,0}, \quad \text{and} \quad \mathbb{E}[u(\omega, \mathbf{x})] = \mathbb{E}\left[\sum_{i=0}^{N_{PC}} \hat{u}_i(\mathbf{x})\psi_i(\boldsymbol{\xi})\right] = \hat{u}_0(\mathbf{x}),$$

where the mean of the solution is equivalent to the first coefficient of the expansion.

Furthermore, each element of the covariance matrix can be approximated by a weighted sum involving the products of all the coefficients except the first one \hat{u}_0 , where the weights correspond to the polynomial stochastic norms $\mathbb{E}[\psi_i^2]$:

$$(14) \quad \begin{aligned} \text{Cov}[u(\omega, \mathbf{x}), u(\omega, \mathbf{y})] &= \mathbb{E}\left[\left(\sum_{i=0}^{N_{PC}} \hat{u}_i(\mathbf{x})\psi_i(\boldsymbol{\xi}) - \hat{u}_0(\mathbf{x})\right)\left(\sum_{i=0}^{N_{PC}} \hat{u}_i(\mathbf{y})\psi_i(\boldsymbol{\xi}) - \hat{u}_0(\mathbf{y})\right)\right] \\ &= \sum_{i=1}^{N_{PC}} \hat{u}_i(\mathbf{x})\hat{u}_i(\mathbf{y})\mathbb{E}[\psi_i^2]. \end{aligned}$$

The straightforward computation of the statistical moments from the gPC surrogate model represents a key advantage of the SSFEM pipeline. Indeed, both the gPC solution statistical analysis and PDF reconstruction are facilitated, since the first can now be performed through a proper combination of the coefficients, and the latter by sampling the solution polynomial expansion, evaluating the polynomials at a sample of their basic random variables $\boldsymbol{\xi}$.

5. A REVISITED BENCHMARK IN FLUID-DYNAMICS: THE COANDĂ EFFECT

Let $\mathcal{D} \in \mathbb{R}^2$ be the bounded domain representing the sudden-expansion channel in Figure 3.

We consider the steady incompressible Navier-Stokes equations described by the PDE:

$$(15) \quad \begin{cases} -\mu\Delta\mathbf{v} + \mathbf{v} \cdot \nabla\mathbf{v} + \nabla p = 0 & \text{in } \mathcal{D}, \\ \nabla \cdot \mathbf{v} = 0 & \text{in } \mathcal{D}, \end{cases} \quad \text{with} \quad \begin{cases} \mathbf{v} = \mathbf{v}_{\text{in}} & \text{on } \Gamma_{\text{in}}, \\ \mathbf{v} = 0 & \text{on } \Gamma_{\text{wall}}, \\ -p\mathbf{n} + (\mu\nabla\mathbf{v})\mathbf{n} = 0 & \text{on } \Gamma_{\text{out}}, \end{cases}$$

where the unknown state of the fluid (\mathbf{v}, p) , encompasses its velocity $\mathbf{v} = (v_x, v_y)$ and pressure p normalized over a constant density, where v_x and v_y stand respectively for the velocity's horizontal and vertical components. The imposed boundary conditions entail a stress-free condition on the velocity at the outlet Γ_{out} , with the outer normal denoted as $\mathbf{n} = (n_{x_1}, n_{x_2})$, a no-slip homogeneous Dirichlet boundary condition on Γ_{wall} , and a non-homogeneous Dirichlet boundary condition $\mathbf{v}_{\text{in}}(x_1, x_2) = [20(5 - x_2)(x_2 - 2.5), 0]$ at the inlet Γ_{in} (see [34] for more details regarding the benchmark).

The parameter μ represents the kinematic viscosity, and plays a crucial role in the behavior of the system. Indeed, being related to the Reynolds number, it balances viscous and inertial forces, originating a symmetry-breaking phenomenon known as the Coandă effect. The unique and stable symmetric branch bifurcates in two asymmetric coexisting configurations, switching its stability property with them at critical values of the fluid's viscosity parameter, and generating the so-called *pitchfork bifurcation*. Its study has relevance in various fields of application, ranging from shape-modeling in aerodynamics to cardiovascular blood-flow in health-care, recently garnering a

substantial body of literature, comprising both experimental and deterministic numerical investigations [43, 15, 34, 10, 26]. In particular, it models the “wall-hugging” tendency of a viscous fluid, which is related to mitral valve regurgitation in the cardiovascular context [34].

For the numerical approximation of the problem, we first need to consider its weak formulation, that reads as: given a parameter $\mu \in \mathcal{P}$, find $(\mathbf{v}, p) \in \mathbb{V}_{\text{in}} \times \mathbb{Q}$ such that

$$(16) \quad \begin{cases} \mu \int_{\mathcal{D}} \nabla \mathbf{v} \cdot \nabla \psi d\mathbf{x} + \int_{\mathcal{D}} (\mathbf{v} \cdot \nabla \mathbf{v}) \psi d\mathbf{x} - \int_{\mathcal{D}} p \nabla \cdot \psi d\mathbf{x}, & \forall \psi \in \mathbb{V}_0 \\ \int_{\mathcal{D}} \pi \nabla \cdot \mathbf{v} d\mathbf{x} = 0, & \forall \pi \in \mathbb{Q}, \end{cases}$$

where $\mathbb{V}_0 = \{\mathbf{v} \in H^1(\mathcal{D}; \mathbb{R}^2) : \psi|_{\Gamma_{\text{wall}} \cup \Gamma_{\text{in}}} = 0\}$, $\mathbb{V}_{\text{in}} = \mathbb{V}_0 \oplus \mathbf{v}_{\text{in}}$, and $\mathbb{Q} = L^2(\mathcal{D})$.

In the next sections, we exploit the weak formulation derived in Equation (16) to recover the bifurcation diagram, both reporting the classical results obtained in the deterministic setting, and describing the new stochastic perspective to the topic, at first testing a non-intrusive Monte Carlo sampling, and finally presenting the SSFEM contribution.

5.1. Deterministic bifurcation analysis. The pitchfork bifurcation originating from the Navier-Stokes system in (15) has been deeply investigated in literature in the deterministic setting, where the kinematic viscosity μ plays the role of the bifurcation parameter, causing the fluid to adhere to adjacent walls.

Specifically, when studying the behavior of the solution of the system while decreasing the kinematic viscosity, the influence of inertia gradually becomes more significant, leading to a symmetry-breaking phenomenon for a critical viscosity value, denoted as μ^* .

Therefore, below this critical threshold, the uniqueness of the solution is lost, and we expect to observe a physically unstable symmetrical flow configuration alongside two stable asymmetric solutions that display wall-hugging behavior. Notably, these solutions coexist for the same parameter values, a characteristic feature of these kind of bifurcating phenomena.

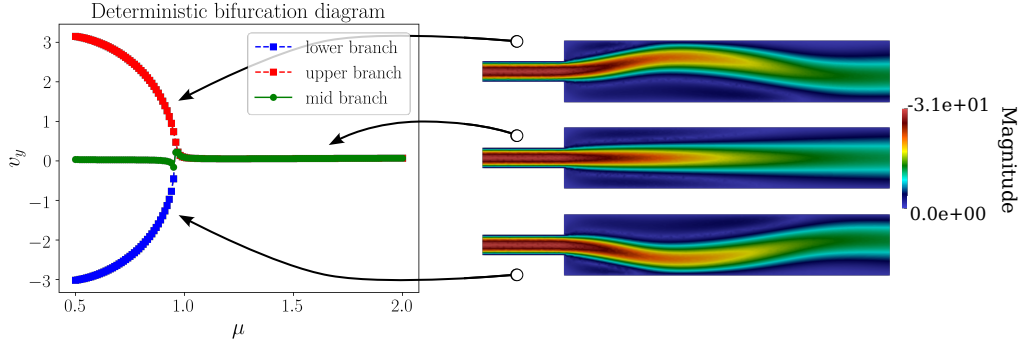


FIGURE 4. Deterministic FEM bifurcation diagram with the corresponding co-existing solutions belonging to the upper, middle and lower branches for $\mu = 0.5$.

To build a bifurcation diagram for the Coandă problem, and thus investigate the evolution of the solution branches, one may choose to examine the behavior of the vertical velocity, the component responsible for breaking the symmetry, at a point along the channel’s symmetry axis \hat{x} , reported in Figure 4. To construct such deterministic diagram, giving a visual information regarding the model’s behavior, one traditionally needs an iterative method involving the deterministic solution of the problem in (15) recovered via some high-fidelity numerical solver. Here, μ has been considered as a known parameter, varying uniformly in the parametric range $\mathbb{P} = [0.5, 2]$ with a step size $\Delta\mu = 0.01$. For this reason, recovering the plot in Figure 4 is complex and costly, as involves a continuation strategy to properly select the initial guess for the nonlinear solver at each new parameter value.

Consistently with the results in literature we can see that, within this parametric/geometry context, the bifurcation occurs at $\mu^* \approx 0.96$. Nevertheless, towards a more realistic and complex scenario, from now on the properties of the branching behavior in a stochastic setting are presented, along with the important computational reduction they bring in the bifurcation point detection and bifurcation diagram construction.

5.2. A non-intrusive approach: Monte Carlo sampling. As anticipated in Section 3.3, a sample-based approach to bifurcation problems could be misleading, providing only partial information about the system’s behavior when any a-priori assumption on the potential multiplicity of the existing branches is made. Indeed, without exploiting ad-hoc techniques such as the deflation method [20], there are no guarantees that the nonlinear solver is able to find samples of the solution equally distributed on the possible branches. For instance, approaching the problem via MC simulations, or similar non-intrusive methodologies, one collects an ensemble of solutions by repeatedly solving the system for different values of the stochastic parameters, without obtaining any assurance on the completeness of the analysis.

Therefore, as a first result regarding possible stochastic approaches to bifurcation problems, we empirically prove this argument to justify the need of intrusive methods when assuming no previous knowledge of the system. We thus treat the viscosity as a normally distributed random variable $\mu \sim \mathcal{N}(0.9, 0.001)$ centered at a point of the parameter space where the bifurcation has already occurred, and we draw 300 samples from such parameter distribution, solving the nonlinear system and collecting an ensemble of solutions.

As shown in Figure 5a, if the nonlinear solver initialization is not exploiting any prior knowledge regarding the possible states, so the initial guess is set to zero, the variance obtained from the collected ensemble has small magnitude in the whole domain. On the other hand, as it can be seen in Figure 5b, if we incorporate some knowledge by means of a continuation approach for the initialization of the Newton-Krylov method, the variance clearly shows a different behavior with an increased magnitude, concentrating in the expansion-region of the channel where the bifurcation is mostly affecting the flow.

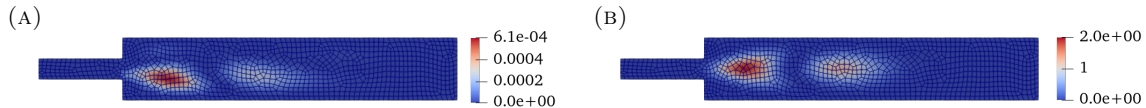


FIGURE 5. Variance of v_y computed via MC simulation of 300 samples with $\mu \sim \mathcal{N}(0.9, 0.001)$ on a quadrilateral grid of 1275 nodes, (a) fixed and (b) ad-hoc knowledge-based initialization.

As a further confirmation of the need for additional knowledge in the non-intrusive approach, we can study the actual samples from the grid points realizing the maximum value of the variance in both cases. In Figure 6a, we see that the higher variance only comes from a linear trend, while in Figure 6b, corresponding to the ad-hoc initialization of the solver, we observe a multi-valued map identifying the three branches in the deterministic bifurcation diagram of Figure 4.

Thus, even if sample-based approaches could be of easier interpretation and implementation, they lack of reliability in the non-uniqueness regime, and require some computationally expensive continuation methods. On the other hand, performing a sample-based stochastic simulation enlarging the parameter interval of interest could lead to interesting results.

It is the case of Figure 6c, where we assign greater variance to the parameter and perform the MC non-intrusive method with prior knowledge of the existence of three admissible branches. Indeed, in the case of $\mu \sim \mathcal{N}(0.9, 0.2)$, not only the bifurcation diagram topology is reproduced, but an additional bifurcating behaviour can be observed around $\mu = 0.5$. Therefore, sample-based approaches to bifurcating problems do not guarantee an accurate prediction of the complete solution manifold, nonetheless they could serve to non-intrusively discover new admissible branches [32, 33, 49].

However, here we are interested in the numerical capabilities of accurately inferring information on the deterministic bifurcation diagram given no prior knowledge of the solution manifold. Following this path, in the next section we discuss the application of the SSFEM intrusive approach to the Navier-Stokes equations with stochastic viscosity.

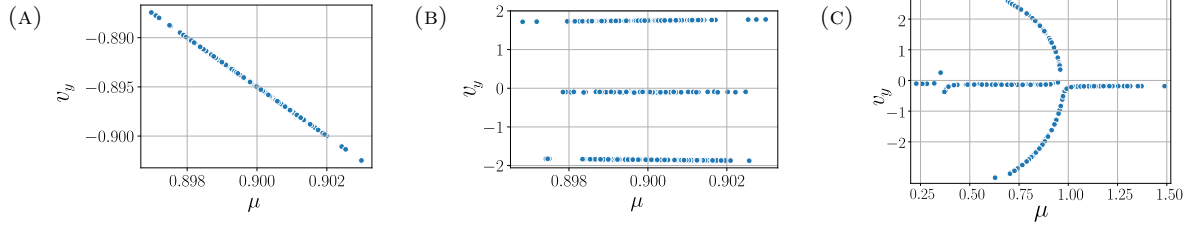


FIGURE 6. Monte Carlo samples of v_y at the point of maximum variance with $\mu \sim \mathcal{N}(0.9, 0.001)$ for Figures 5a and 5b in (a) and (b) respectively, and with $\mu \sim \mathcal{N}(0.9, 0.2)$ in (c).

5.3. SSFEM approach: random viscosity parameter. Having highlighted the issues when dealing with non-intrusive approaches, we proceed exploring the evolution of the system via the SSFEM pipeline presented in Section 4. In order to study the behaviour of the solution in a small neighborhood of the viscosity parameter, we consider μ as the random variable following a given distribution with mean $\bar{\mu}$. We can write its K-L expansion (4) as $\mu = \bar{\mu} + \sigma\bar{\xi}$, where $\pi_1(\mathbf{x}) = 1$. In the case of $\mu \sim \mathcal{N}(\bar{\mu}, \sigma)$ one has $\bar{\xi}_1 = \bar{\xi} \sim \mathcal{N}(0, 1)$ and $\lambda_1 = \sigma^2$.

Thus, by expanding the unknowns of the problem in (16) we can write:

$$(17) \quad \mathbf{v}(\mathbf{x}, \omega) = \sum_{i=0}^{N_D^v} \sum_{j=1}^{N_{PC}^v} \mathbf{v}_{i,j} \phi_i^v(\mathbf{x}) \psi_j^v(\boldsymbol{\xi}(\omega)), \quad \text{and} \quad p(\mathbf{x}, \omega) = \sum_{i=0}^{N_D^p} \sum_{j=1}^{N_{PC}^p} p_{i,j} \phi_i^p(\mathbf{x}) \psi_j^p(\boldsymbol{\xi}(\omega)),$$

where the superscripts denote quantities related to the velocity and pressure fields. This way, the system can be expressed in the generic form of Equation (12). In particular, both equations in the weak formulation (16) can be expanded both in the FEM space via the test functions $\{\phi_n^v(\mathbf{x})\}_{n=1}^{N_D^v}$, $\{\phi_n^p(\mathbf{x})\}_{n=1}^{N_D^p}$, and in the probabilistic one with $\{\psi_m^v(\boldsymbol{\xi})\}_{m=1}^{N_{PC}^v}$, $\{\psi_m^p(\boldsymbol{\xi})\}_{m=1}^{N_{PC}^p}$, $\forall n \in \{1, \dots, N_D^v\}, \forall m \in \{1, \dots, N_{PC}^v\}$, as follows:

$$(18) \quad \left\{ \begin{array}{l} \sum_{k=0}^1 \sum_{i=0}^{N_D^v} \sum_{j=1}^{N_{PC}^v} \mathbf{v}_{i,j} \int_{\mathbb{R}} \sqrt{\lambda_k} \xi_k \psi_j^v(\boldsymbol{\xi}) \psi_m^{(v)}(\boldsymbol{\xi}) d\nu_{\boldsymbol{\xi}} \int_D \nabla \phi_i^v(\mathbf{x}) \cdot \nabla \phi_n^v(\mathbf{x}) d\mathbf{x} \\ + \sum_{i=0}^{N_D^v} \sum_{j=1}^{N_{PC}^v} \sum_{l=0}^{N_D^v} \sum_{h=1}^{N_{PC}^v} \mathbf{v}_{i,j} \mathbf{v}_{l,h} \int_{\mathbb{R}} \psi_j^v(\boldsymbol{\xi}) \psi_h^v(\boldsymbol{\xi}) \psi_m^v(\boldsymbol{\xi}) d\nu_{\boldsymbol{\xi}} \int_D (\phi_i^v(\mathbf{x}) \cdot \nabla \phi_n^v(\mathbf{x})) \phi_l^v(\mathbf{x}) d\mathbf{x} \\ - \sum_{i=0}^{N_D^p} \sum_{j=1}^{N_{PC}^p} p_{i,j} \int_{\mathbb{R}} \psi_j^p(\boldsymbol{\xi}) \psi_m^v(\boldsymbol{\xi}) d\nu_{\boldsymbol{\xi}} \int_D \phi_i^p(\mathbf{x}) \nabla \cdot \phi_n^v(\mathbf{x}) d\mathbf{x} = 0, \\ \sum_{i=0}^{N_D^v} \sum_{j=1}^{N_{PC}^v} \mathbf{v}_{i,j} \int_D \nabla \cdot \phi_i^v(\mathbf{x}) \phi_n^p(\mathbf{x}) d\mathbf{x} \int_{\mathbb{R}} \psi_j^v(\boldsymbol{\xi}) \psi_m^p(\boldsymbol{\xi}) d\nu_{\boldsymbol{\xi}} = 0. \end{array} \right.$$

Thanks to the SSFEM expansion, we rewrite the weak formulation (16) in the compact form

$$(19) \quad \begin{cases} \mathbf{A}^T \cdot \mathbf{U} \cdot (\mathbf{E}^{(0)} + \mathbf{E}^{(1)}) + \mathbf{I} - \mathbf{C}^T \cdot \mathbf{Q} \cdot \mathbf{G} = \mathbf{0}, \\ \mathbf{D}^T \cdot \mathbf{U} \cdot \mathbf{H} = \mathbf{0} \end{cases}$$

where we denoted with $\mathbf{U} \in \mathbb{R}^{N_D^v \times N_{PC}^v}$ and $\mathbf{Q} \in \mathbb{R}^{N_D^p \times N_{PC}^p}$, respectively, the unknown coefficients for the velocity and pressure fields. Denoting with \odot the Hadamard product, the FEM and stochastic matrices can be defined in Equations (20) and (21), respectively as

$$(20) \quad \begin{aligned} A_{j,n} &= \int_{\mathcal{D}} \nabla \phi_j^v \cdot \nabla \phi_n^v d\mathbf{x}, & B_{n,j,h} &= \int_{\mathcal{D}} (\phi_j^v \cdot \nabla \phi_h^v) \phi_n^v d\mathbf{x}, & C_{j,n} &= \int_{\mathcal{D}} \phi_j^p \nabla \cdot \phi_n^v d\mathbf{x}, \\ D_{j,n} &= \int_{\mathcal{D}} \nabla \cdot \phi_j^v \phi_n^p d\mathbf{x}, & I_{n,m} &= (\mathbf{U}^T \cdot \mathbf{B}_n \cdot \mathbf{U}) \odot \mathbf{F}_m, \end{aligned}$$

$$(21) \quad \begin{aligned} E_{i,m}^{(0)} &= \int_{\mathbb{R}} \sqrt{\lambda_0} \xi_0 \psi_i^v \psi_m^v d\nu_{\xi}, & E_{i,m}^{(1)} &= \int_{\mathbb{R}} \sqrt{\lambda_1} \xi_1 \psi_i^v \psi_m^v d\nu_{\xi}, & F_{m,l,i} &= \int_{\mathbb{R}} \psi_i^v \psi_l^v \psi_m^v d\nu_{\xi}, \\ G_{i,m} &= \int_{\mathbb{R}} \psi_i^p \psi_m^v d\nu_{\xi}, & H_{i,m} &= \int_{\mathbb{R}} \psi_i^v \psi_m^p d\nu_{\xi}. \end{aligned}$$

As concerns the imposition of the boundary conditions defined in the general formulation of the problem (15), we identify the inlet/wall nodes belonging to Γ_{in} and Γ_{wall} , and we enforce them strongly by directly updating the matrices. We have now everything in place to present the statistical analysis of the bifurcating problem.

6. RESULTS

In this section, we discuss the numerical results of the SSFEM pipeline when applied to the Navier-Stokes equations modelling the Coandă bifurcation problem. Consistently with other studies in the deterministic setting [34, 26], we exploit the vertical component of the velocity field to discuss the non-uniqueness feature of the model. We start presenting its statistical moments in relation with the ones assigned to the viscosity. Therefore, in this first analysis, the viscosity parameter is defined as a Gaussian distribution centered near the known bifurcation point with a small variance. This specific choice has been made to study the system's response to limited perturbations, in the case in which the multiple coexisting branches (see Figure 4) are still reasonably close to each other.

Successively, we discuss the stability of the PC solution with respect to different parametric instances, in particular to the coarseness and symmetry of the computational grid. We show the effect of the prior distribution associated to the viscosity parameter on the solution, investigating the different polynomial expansions on the sought approximated solution. Finally, we perform a deeper investigation of the role played by the polynomial coefficients in the PC expansion. We extend the statistical analysis of the solution to multiple viscosity values far from the bifurcation point, and discuss the discovered strict and surprising relationship between the PC representation of the solution and its deterministic bifurcation diagram.

The numerical simulations are conducted thanks to a SSFEM implementation based on the deal.II library. The code³ is parallelized to enable faster computations on larger meshes, and enriched with additional functions enabling the extension of the classical deterministic FEM, e.g. representing the unknowns as SSFEM matrices instead of FEM vectors. The space discretization has been carried out using the Taylor-Hood ($\mathbb{P}_2\text{-}\mathbb{P}_1$) elements.

6.1. Statistical moments around the bifurcation point. As a first step, we are interested in understanding whether or not the statistical moments inferred from the PC representation of the velocity solution (see Section 4.1) are informative on its bifurcating behaviour.

To this aim, we start performing the SSFEM computation assigning a Gaussian distribution to the viscosity $\mu \sim \mathcal{N}(\bar{\mu}, \sigma)$, where the mean is located in the non-uniqueness regime of the parametric space. Therefore, following the intuitive interpretation of a bifurcating behaviour where drastic changes follow small variation of the parameter, we apply a small stochastic perturbation to the kinematic viscosity μ . In particular, we expect that the stochastic solution exhibits greater variance at the spatial coordinates for which the discrepancy between the coexisting deterministic solutions is maximized.

³<https://github.com/ICGonnella/SSFEM-Coanda-Effect.git>

In Figure 7 we show the mean and the variance of v_y computed relying only on a linear polynomial expansion of the velocity. Interestingly, it can be noticed that the grid point corresponding to the highest variance value is located in the post-inlet region, where the vertical components of the admissible velocity solutions break the symmetry. Therefore, having this statistical information, one can easily locate the point of maximum discrepancy of the coexisting solutions directly in the computational domain.

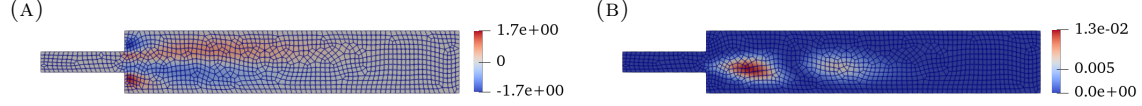


FIGURE 7. SSFEM statistics (a) mean and (b) variance on a quadrilateral grid of 1275 nodes, obtained using a linear PC expansion ($N_{PC} = 2$) and $\mu \sim \mathcal{N}(0.9, 0.001)$.

Nevertheless, from the above variance plots it is not possible to distinguish between a bifurcating behavior of the solution, and a simple a high variability induced by several other factors. In order to investigate this difference, possibly encoded in the SSFEM solution, we search for some insights on its polynomials. More precisely, we analyse the shape of the polynomial random variables corresponding to the evaluation of the stochastic process at a specific domain point, in particular in the regions of the domain showing higher variance.

We recall that an evaluation of the solution stochastic process at a specific point of the domain corresponds to the random variable resulting from the composition of the polynomial function itself and the basic random variables. Thus, by defining the *sampling zone* as the subset of $\text{supp}(\xi)$ at which the 99% of the measure ν_ξ is concentrated (e.g. it corresponds to the interval $(-3, 3)$ for standard normal basic random variables ξ), we can conclude that the relevant local extrema for the solution are actually the ones found in this region. Therefore, the shape of polynomials must be studied in the sampling zone of the ξ variables. In particular, the main feature we want to discuss now is the possible correlation between the minima and maxima of the polynomials and the presence of a bifurcating behaviour.

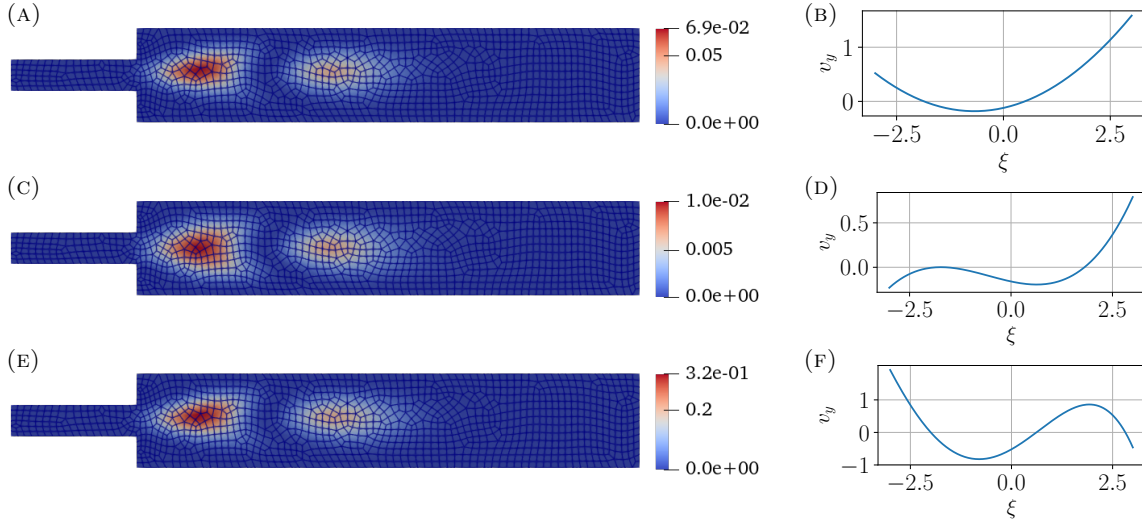


FIGURE 8. SSFEM results on a quadrilateral grid of 1275 nodes with $\mu \sim \mathcal{N}(0.9, 0.001)$. Variance magnitude and solution at \bar{x} , for $N_{PC}=3$ (a)(b), $N_{PC}=4$ (c)(d), and $N_{PC}=5$ (e)(f).

To explore further this intuition, we proceed with the analysis of the velocity variance for increasing polynomial degree. As it can be seen in Figures 7, 8, the variance magnitude tend to increases

in absolute value as the polynomial degree increases, but remains localized at the same grid points. This consistency w.r.t. the increasing capability of the polynomial expansion confirms the ability of the PC surrogate model to accurately reveal the coordinates at which a relevant change in the solution occurs.

Moreover, along with the variance plots, we show the shapes of the polynomials for the high variance domain point $\bar{x} = (15, 3.75)$ belonging to the horizontal symmetry axis. It can be noticed that up to degree two there is no evidence of bifurcating behavior, as only one local extrema appears. Instead, when reaching degree three, multiple local extrema are visible in the sampling area, whose values for degree four (see Figure 8f) seem to tend to the values of the two stable solution branches in that specific domain point (see Figure 4).

Therefore, a correlation between the value of the local extrema in the sampling region and the branching solutions is revealed, suggesting that a bifurcating behaviour is characterized by the joint occurrence of both a high variance and multiple local extrema for the solution's PC representation. Moreover, one can note that the high-variance region keeps improving its symmetry w.r.t. the horizontal axis starting from degree two, while for degree one (see Figure 7b) it is not perfectly centered yet. This, together with the progressive adjustment of the peaks values versus the stable branches values (from Figure 8d to Figure 8f), remarks even more the dependence of the PC representation's accuracy of the bifurcating phenomenon to the polynomial degree considered.

In order to give a complete overview on the role of the local extrema, in Figure 9 the PDF of the vertical component of the velocity solution is reconstructed thanks to its PC representation, as a large number of samples can be collected and used for the Kernel Density Estimation (KDE) [41]. Two peaks can be observed at the two local extrema of the correspondent polynomial of Figure 8f, around the values $\{-1, 1\}$. Indeed, as anticipated before, samples of the solution are obtained by repeatedly applying the polynomial function to samples collected from a normal random variable $\xi \sim \mathcal{N}(0, 1)$. Thus, it is reasonable that the polynomial samples are concentrated around the local maxima and minima values, since those are points of lower gradient of the function. Actually, for this very reason we observe a higher peak around -1 in the density plot, as the abscissa of the corresponding local minimum is close to zero, and thus significantly more frequent in the sampling process of ξ .

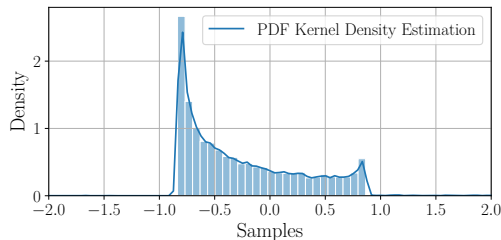


FIGURE 9. KDE of the velocity PDF for $\mu \sim \mathcal{N}(0.9, 0.001)$ at point \bar{x} of maximum variance.

Given this preliminary analysis on the influence of a small Gaussian noise applied to the viscosity parameter, we aim at investigating the influence of assuming different a-priori distributions. We conduct such analysis in the following section, where we consider uniform distributions for the viscosity, and the impact of different computational meshes.

6.2. Influence of distributions and mesh discretizations. Motivated by the asymmetry of the peaks in Figure 9, we report the variance and the correspondent polynomial analysis in case of $\mu \sim \mathcal{U}(a, b)$, where a, b are chosen to have the distribution centered at value 0.9 with same variance as in the previous section. When dealing with uniform basic random variables ξ , the corresponding orthogonal polynomials are the Legendre ones, for which the sampling region is given by $\xi \sim \mathcal{U}(-1.73, 1.73)$, with zero mean and variance equals to one.

Consistently with the former results, as we can see from Figure 10, also for such viscosity distribution the variance of the vertical velocity is concentrated in the post-inlet region. Given the different PC expansion, what may differ is instead the polynomials shape, which is reported for the same domain point \bar{x} belonging to the horizontal symmetry axis as in the previous section. Indeed, this time the number of local extrema increases until degree four (see Figure 10f), arriving at a maximum of three peaks, also maintained by the degree five PC representation (see Figure 10h). Also in this case the extrema change while increasing the PC degree, with values in $\{-2, 0, 2\}$, which accurately correspond to the three solution branches of the deterministic case (two stable and one unstable).

Moreover, sampling of the polynomials according to a uniform ξ lead to Figure 13a, where three evident peaks are visible, corresponding precisely to the three extrema of the polynomial in Figure 10h. We remark that a minor peak seems also to be present for a viscosity value larger than 2. Nevertheless, this is clearly negligible with respect to the others, as it derives from the maximum of Figure 10h barely appearing at the left margin of the sampling region. Thus, by assigning a uniform distribution to μ , which is not strictly peaked on the mean value as in the Gaussian case, Legendre polynomials allow inferring the unstable branch and capturing a larger variance of the solution.

Furthermore, we investigate the influence of the computational mesh exploited for the bifurcation detection. Indeed, until now we have worked with unstructured grids with a relatively coarse mesh. We now report the variance of the vertical velocity together with the polynomial solution for the case of structured and unstructured dense grids, embedding some notion of symmetry in the discretization of the problem.

In particular, in Figure 11 we show the case of a structured highly symmetric grid, for which the variance of the vertical velocity changes significantly. Moreover, observing Figure 11b, no local extrema are visible in the corresponding polynomials evaluated at \bar{x} , suggesting that no bifurcating behaviour is detected. This is due to the influence of the mesh on the bifurcation analysis, as already observed in the deterministic case [23, 31].

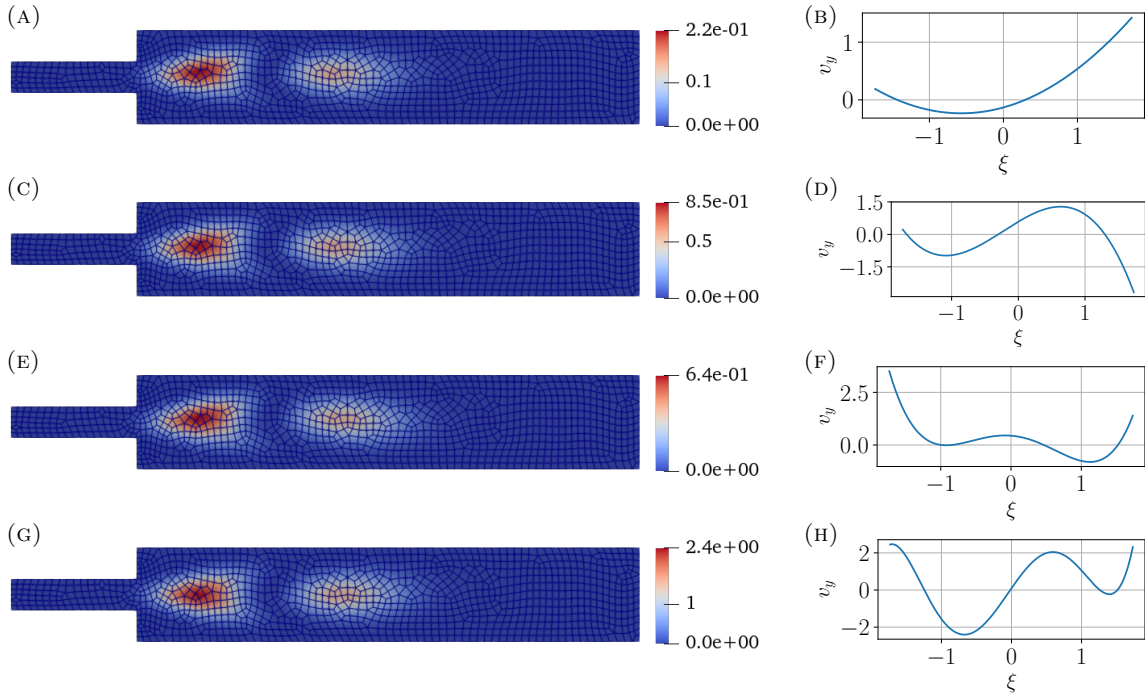


FIGURE 10. SSFEM results with $\mu \sim \mathcal{U}(0.845, 0.955)$. Variance magnitude and solution at \bar{x} , for $N_{PC} = 3$ (a)(b), $N_{PC} = 4$ (c)(d), $N_{PC} = 5$ (e)(f), $N_{PC} = 6$ (g)(h).

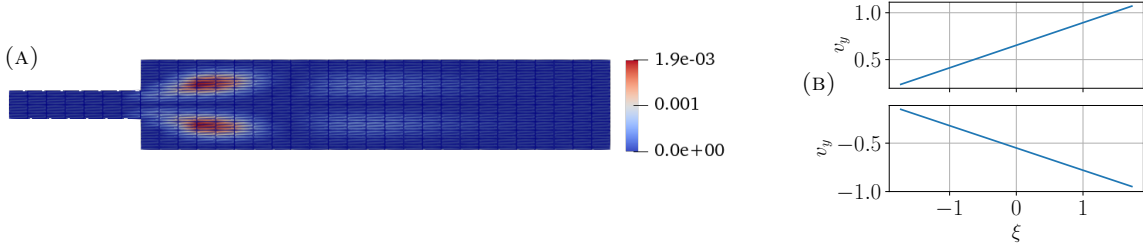


FIGURE 11. SSFEM results on a quadrilateral symmetric grid of 935 nodes with $\mu \sim \mathcal{U}(0.845, 0.955)$: (a) variance magnitude, and (b) solution at \bar{x}_1 and \bar{x}_2 .

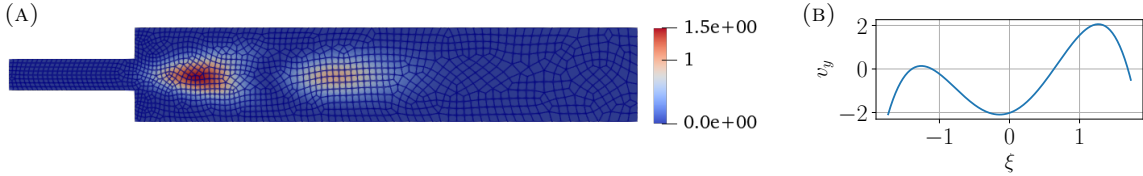


FIGURE 12. SSFEM results on a quadrilateral grid of 1541 nodes with $\mu \sim \mathcal{U}(0.845, 0.955)$: (a) variance magnitude, and (b) solution at \bar{x} .

On the other hand, when dealing with dense unstructured grids, as the one displayed in Figure 12, the bifurcating behaviour is clearly detected, and the polynomial shape is able to better capture the solution branches already at degree four.

Indeed, by considering a better discretization of the computational domain, we improved the SSFEM performance w.r.t. the results in coarser grid, that reached the same results only exploiting polynomials of degree five.

To complete the discussion, we refer to Figure 13b the reconstructed PDF corresponding to the last dense unstructured grid, showing once again the emergence of the three peaks in the solution PDF, corresponding to the three solution branches. This is put in comparison with the PDF emerging from Figure 10g in the case of a coarser unstructured grid, reported in Figure 13a.

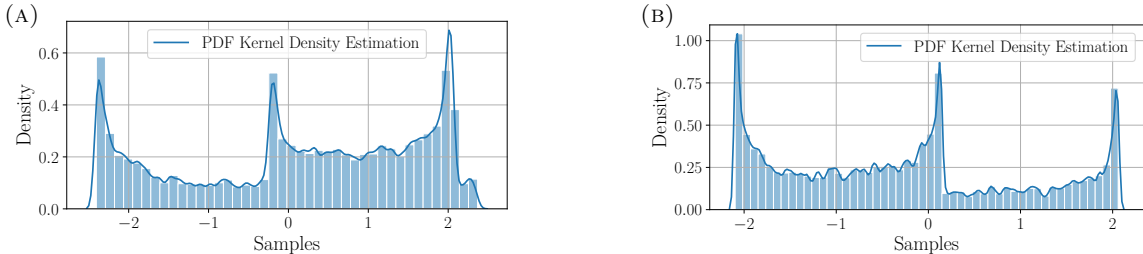


FIGURE 13. Kernel Density Estimation of the velocity PDF at the domain point of maximum variance for $\mu \sim \mathcal{U}(0.845, 0.955)$, for non-symmetric meshes of (a) 1275 and (b) 1541 nodes.

6.3. Deterministic bifurcation diagram inference. In this final section, we want extend the previous analysis for different viscosity regimes, thus going in the direction of having zero knowledge regarding the bifurcation and re-discovering a-posteriori the phenomenon.

First, we are interested in checking the behavior of the velocity variance in the uniqueness regime. In Figure 14 the SSFEM results are shown for $\mu \sim \mathcal{U}(1.245, 1.355)$, thus quite far from the bifurcation point. When the uniqueness of the deterministic solution is ensured, the variance is significantly

lower (about three orders of magnitude) than the one observed in the non-uniqueness regime for μ centered in 0.9.

When moving the viscosity value towards the bifurcation point, as expected, the variance increases as shown in Figure 15 for $\mu \sim \mathcal{U}(0.945, 1.055)$. Nevertheless, in both cases the corresponding polynomials, evaluated in the domain points of maximum variance, do not present multiple local extrema. This is consistent with our interpretation, confirming the variance increase approaching the bifurcating regime, while providing the expected information regarding the connection between local maxima and number of branches.

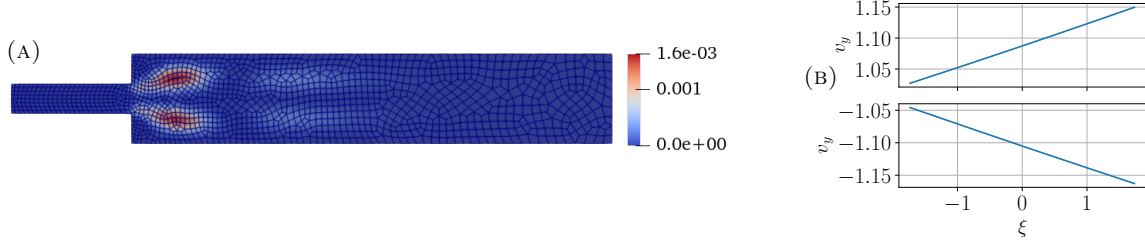


FIGURE 14. SSFEM results on a quadrilateral grid of 1541 nodes with $\mu \sim \mathcal{U}(1.245, 1.355)$: (a) variance magnitude, and (b) solution at \bar{x}_1 and \bar{x}_2 .

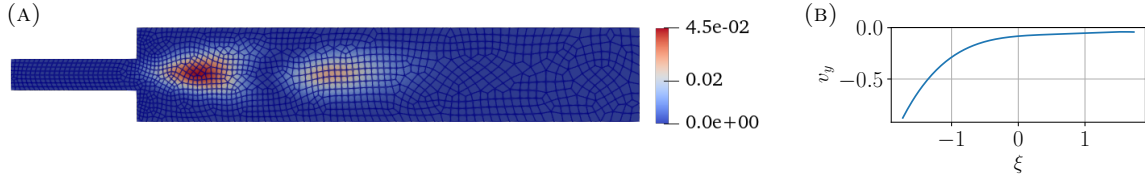


FIGURE 15. SSFEM results on a quadrilateral grid of 1541 nodes with $\mu \sim \mathcal{U}(0.945, 1.055)$. Variance magnitude (a), and solution at \bar{x} (b).

Towards a complete investigation of the bifurcation diagram, we are interested in the possibility of reconstructing the branches for any value of viscosity, without relying on any prior information. To this end, we perform the same analysis for viscosity values below the critical bifurcation point μ^* . In particular, we report the results of the SSFEM computations for $\mu \sim \mathcal{U}(0.745, 0.855)$ and $\mu \sim \mathcal{N}(0.645, 0.755)$ in Figure 16. The magnitude of the variance increases with respect to Figure 12 where we considered $\mu \sim \mathcal{U}(0.845, 0.955)$, and progressively becomes higher as the viscosity mean decreases. Indeed, this can be explained with the progressive separation of the branches already in the deterministic bifurcation diagram.

Expansion polynomials can be retrieved and sampled according to the distribution of their basic random variables, and are shown in Figures 16b and 16d.

We remark that, in the cases where the branches of the solution progressively separate, the computation of the PC coefficients is typically more expensive initializing the nonlinear solver with a zero guess. Moreover, more dense grids are in general required for a higher precision. On the other hand, following the interpretation given to the polynomials, higher coefficients must be achieved to fully exploit the capability of the surrogates, requiring increasingly intense computations.

By looking at the polynomials, SSFEM is also able to detect three local extrema in the sampling region for quite low viscosity values. Moreover, their values follow the peaks identified by the trend of the branches in the deterministic diagram. Nevertheless, given the difficulties highlighted before, the symmetry between positive and negative values for the two stable branches is not exactly recovered with this mesh, as the wall-hugging bottom flow is identified but not accurately reached in magnitude. Nevertheless, the unstable symmetric branch seems to be always recovered.

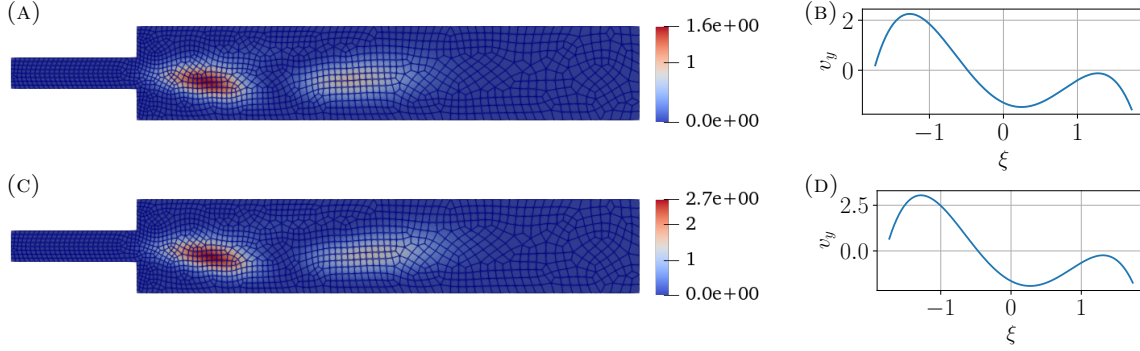


FIGURE 16. SSFEM results on a grid of 1541 nodes: variance magnitude and solution at \bar{x} , for $\mu \sim \mathcal{U}(0.745, 0.855)$ in (a)(b) and $\mu \sim \mathcal{U}(0.645, 0.755)$ in (c)(d).

We can exploit the results obtained to visualize a probabilistic version of the bifurcation diagram. In Figure 17, we report this comparison, highlighting with different markers the admissible solutions for different viscosity parameters. By displaying the PDF plot related to the solution of the stochastic PDEs for the viscosity perturbed around these values, we observe that the branches of the solution are exactly recovered in the case of $\mu = 0.9$, and that for $\mu = 1.0$ the density of the solution is concentrated on a single value, corresponding to the unique solution. Even when considering viscosity values in the “strong” bifurcation regime, namely $\mu = 0.7$ and $\mu = 0.8$, the evolution of the branches is followed, although the lower branch is not perfectly recovered in its symmetry due to convergence difficulties.

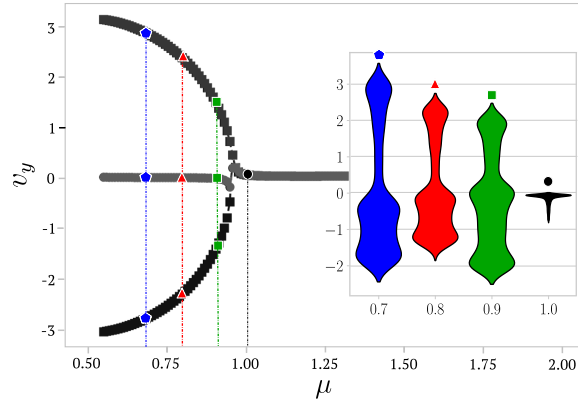


FIGURE 17. SSFEM probabilistic bifurcation diagram for different viscosity values.

This analysis confirms the potentialities in investigating complex bifurcating phenomena under the stochastic point of view via probabilistic-aware surrogate approaches, as a way of inferring features of the deterministic model through stochastic perturbations. Moreover, it also opens for a research path to address the performance of the PC expansion accuracy w.r.t. the properties of the mesh and the type/order of the polynomials.

7. CONCLUSIONS AND PERSPECTIVES

In this work, we propose a numerical stochastic-perturbation approach to deterministic bifurcation problems. We develop and implement an intrusive pipeline based on the Spectral Stochastic Finite Element Method to retrieve the Polynomial Chaos expansion coefficients of the probabilistic solution, and we find that, under little perturbations of the bifurcation parameter, it successfully encodes accurate information about the deterministic bifurcation diagram.

For what concerns the PC surrogate model of a stochastic bifurcating PDE, we show the strict relation between the branches of coexisting solutions, and the local extrema of the corresponding PC functions. Indeed, the number of local extrema in the sampling region demonstrates a correspondence with the number of solution branches for the specific parameter value at which the distribution is centered. Moreover, the value of such local extrema tend to concentrate around the values of the branches, leading to the formation of clusters of points around them when the solution is sampled.

Therefore, we show that such intrusive stochastic approach overcomes an important issue arising in the computational bifurcating context, as it does not require any prior knowledge about the solution branches to give back valid information about the solution manifold. Indeed, in the non-intrusive case, in order to compute samples of the non-unique parametric solution some prior information about the bifurcating behaviour is required to be embedded in the sampling strategy. This precaution is essential to allow the numerical solver to converge to different branches, and thus to provide a complete overview of the solution manifold via a meaningful and representative ensemble of admissible configurations. As a result, SSFEM offers a significant advantage by being independent of problem-specific initialization, while still providing a precise representation of the complete solution manifold.

On the other hand, from a strictly computational point of view, the SSFEM intrusive approach is expensive due to the dimension of the system to be solved for high polynomial degrees. This poses new computational challenges, which can be mitigated through ad-hoc convergence strategies and preconditioning methods, as shown in previous works also addressing the Navier-Stokes equations [44, 28]. Therefore, important improvements could be achieved, enabling faster computation of higher order coefficients and allowing for the analysis of more complex behaviours, such as the case of higher Reynolds numbers in the Navier-Stokes setting, where successive bifurcations emerge. Solutions to such computational bottle-neck could be given also by the exploitation of well-known reduction strategies different from FEM in the domain space, which could thus be enriched with the PC representation of the probability space and used to solve stochastic PDEs.

Moreover, additional investigations could focus on the source of stochasticity in the system. For instance, random initial and/or boundary conditions may play an important role in the evolution of the system for time-dependent problems, and this could be used to infer a probabilistic overview of the model's behaviour in time.

Finally, given the reliability of the PC surrogate model for the probability distribution of the solution, it is worth exploring a Bayesian approach to the bifurcation problem starting from this prior assumption, possibly following the framework proposed in [22] and adapting it to the polynomial basis. Indeed, incorporating real data into the analysis could be particularly important to model the complex behaviour of a real-world parametric system, as it could bring model's improvements in its reality reproduction capability.

ACKNOWLEDGMENT

The authors thank Pasquale Claudio Africa for the fruitful discussions and fundamental support with the deal.II implementation of the method, and acknowledge the support by Gruppo Nazionale di Calcolo Scientifico (INdAM-GNCS). This work has been conducted within the research activities of the consortium iNEST (Interconnected North-East Innovation Ecosystem), Piano Nazionale di Ripresa e Resilienza (PNRR) – Missione 4 Componente 2, Investimento 1.5 – D.D. 1058 23/06/2022, ECS00000043, supported by the European Union's NextGenerationEU program.

REFERENCES

- [1] E. L. Allgower and K. Georg. *Introduction to numerical continuation methods*. SIAM, 2003.
- [2] A. Ambrosetti and G. Prodi. *A Primer of Nonlinear Analysis*. Cambridge Studies in Advanced Mathematics. Cambridge University Press, 1995.
- [3] N. Arcozzi, M. Campanino, and G. Giambartolomei. The Karhunen-Loeve theorem. Master's thesis, University of Bologna, 2015.
- [4] L. Arnold. *Random Dynamical Systems*. Springer, Berlin, Heidelberg, 1998.

- [5] L. Arnold and P. Boxler. *Stochastic bifurcation: instructive examples in dimension one*, pages 241–255. Birkhäuser Boston, Boston, MA, 1992.
- [6] I. Babuška, F. Nobile, and R. Tempone. A stochastic collocation method for elliptic partial differential equations with random input data. *SIAM Journal on Numerical Analysis*, 45(3):1005–1034, 2007.
- [7] P. Benner, A. Cohen, M. Ohlberger, and K. Willcox. *Model Reduction and Approximation: Theory and Algorithms*. SIAM, Society for Industrial and Applied Mathematics, 2017.
- [8] A. Blumenthal, M. Engel, and A. Neamtu. On the pitchfork bifurcation for the Chafee-Infante equation with additive noise. *Probability Theory and Related Fields*, August 2021.
- [9] N. Boullé, P. E. Farrell, and A. Paganini. Control of bifurcation structures using shape optimization. *SIAM Journal on Scientific Computing*, 44(1):A57–A76, 2022.
- [10] J. R. Bravo, G. Stabile, M. Hess, J. A. Hernandez, R. Rossi, and G. Rozza. Geometrically parametrised reduced order models for studying the hysteresis of the Coanda effect in finite element-based incompressible fluid dynamics. *Journal of Computational Physics*, 509:113058, 2024.
- [11] S. L. Brunton, J. L. Proctor, and J. N. Kutz. Discovering governing equations from data by sparse identification of nonlinear dynamical systems. *Proceedings of the national academy of sciences*, 113(15):3932–3937, 2016.
- [12] G. Caloz and J. Rappaz. Numerical analysis for nonlinear and bifurcation problems. In *Handbook of Numerical Analysis*, volume 5 of *Techniques of Scientific Computing (Part 2)*, pages 487–637. Elsevier, 1997.
- [13] R. H. Cameron and W. T. Martin. The orthogonal development of non-linear functionals in series of Fourier-Hermite functionals. *Annals of Mathematics*, 48:385, 1947.
- [14] G. Carere, M. Strazzullo, F. Ballarin, G. Rozza, and R. Stevenson. A weighted POD-reduction approach for parametrized pde-constrained optimal control problems with random inputs and applications to environmental sciences. *Computers & Mathematics with Applications*, 102, 2021.
- [15] W. Cherdron, F. Durst, and J. H. Whitelaw. Asymmetric flows and instabilities in symmetric ducts with sudden expansions. *Journal of Fluid Mechanics*, 84(1):13–31, 1978.
- [16] K. A. Cliffe, A. Spence, and S. J. Tavener. The numerical analysis of bifurcation problems with application to fluid mechanics. *Acta Numerica*, 9:39–131, January 2000.
- [17] D. Coscia, N. Demo, and G. Rozza. Generative adversarial reduced order modelling. *Scientific Reports*, 14(1):3826, 2024.
- [18] R. Crisovan, D. Torlo, R. Abgrall, and S. Tokareva. Model order reduction for parametrized nonlinear hyperbolic problems as an application to uncertainty quantification. *Journal of Computational and Applied Mathematics*, 348:466–489, 2019.
- [19] O. G. Ernst, A. Mugler, H.-J. Starkloff, and E. Ullmann. On the convergence of generalized Polynomial Chaos expansions. *ESAIM: Mathematical Modelling and Numerical Analysis*, 46(2), 2012.
- [20] P. E. Farrell, Á. Birkinsson, and S. W. Funke. Deflation techniques for finding distinct solutions of nonlinear partial differential equations. *SIAM Journal on Scientific Computing*, 37, 2015.
- [21] R. G. Ghanem and P. D. Spanos. *Stochastic Finite Elements: A Spectral Approach*. Springer, New York, NY, 1991.
- [22] M. Girolami, E. Febrianto, G. Yin, and F. Cirak. The statistical finite element method (statfem) for coherent synthesis of observation data and model predictions. *Computer Methods in Applied Mechanics and Engineering*, 375:113533, March 2021.
- [23] M. Hess, A. Alla, A. Quaini, G. Rozza, and M. Gunzburger. A localized reduced-order modeling approach for PDEs with bifurcating solutions. *Computer Methods in Applied Mechanics and Engineering*, 351:379–403, 2019.
- [24] J. S. Hesthaven, G. Rozza, and B. Stamm. *Certified Reduced Basis Methods for Parametrized Partial Differential Equations*. SpringerBriefs in Mathematics. Springer International Publishing, 2015.
- [25] S. Huang, S. Quek, and K. Phoon. Convergence study of the truncated Karhunen-Loève expansion for simulation of stochastic processes. *International Journal for Numerical Methods in Engineering*, 52(9):1029–1043, 2001.
- [26] M. Khamlich, F. Pichi, and G. Rozza. Model order reduction for bifurcating phenomena in fluid-structure interaction problems. *International Journal for Numerical Methods in Fluids*, 94, June 2022.
- [27] C. Kuehn, C. Piazzola, and E. Ullmann. Uncertainty quantification analysis of bifurcations of the Allen-Cahn equation with random coefficients. *arXiv preprint arXiv:2404.04639*, 2024.
- [28] K. Lee, H. C. Elman, and B. Sousedik. A low-rank solver for the Navier-Stokes equations with uncertain viscosity. *SIAM/ASA Journal on Uncertainty Quantification*, 7:1275–1300, 2019.
- [29] M. Liu. Stability and dynamical bifurcation of a stochastic regime-switching predator-prey model. *Journal of Mathematical Analysis and Applications*, 535(1):128096, 2024.
- [30] E. Mirzakhilili and B. I. Epureanu. Probabilistic analysis of bifurcations in stochastic nonlinear dynamical systems. *Journal of Computational and Nonlinear Dynamics*, 14(8), June 2019.
- [31] F. Pichi. *Reduced Order Models for parametric Bifurcation Problems in Nonlinear PDEs*. PhD thesis, Scuola Internazionale Superiore di Studi Avanzati, Trieste, 2020.
- [32] F. Pichi, F. Ballarin, G. Rozza, and J. S. Hesthaven. An artificial neural network approach to bifurcating phenomena in computational fluid dynamics. *Computers & Fluids*, 254:105813, 2023.
- [33] F. Pichi, B. Moya, and J. S. Hesthaven. A graph convolutional autoencoder approach to model order reduction for parametrized pdes. *Journal of Computational Physics*, 501:112762, 2024.

- [34] F. Pichi, M. Strazzullo, F. Ballarin, and G. Rozza. Driving bifurcating parametrized nonlinear PDEs by optimal control strategies: Application to Navier-Stokes equations with model order reduction. *ESAIM: Mathematical Modelling and Numerical Analysis*, 56:1361–1400, 2022.
- [35] M. Pintore, F. Pichi, M. Hess, G. Rozza, and C. Canuto. Efficient computation of bifurcation diagrams with a deflated approach to reduced basis spectral element method. *Advances in Computational Mathematics*, 47, 2020.
- [36] G. Pitton and G. Rozza. On the application of reduced basis methods to bifurcation problems in incompressible fluid dynamics. *Journal of Scientific Computing*, 73(1):157–177, 2017.
- [37] A. Quaini, R. Glowinski, and S. Čanić. Symmetry breaking and preliminary results about a Hopf bifurcation for incompressible viscous flow in an expansion channel. *International Journal of Computational Fluid Dynamics*, 30(1):7–19, 2016.
- [38] A. Quarteroni. *Numerical Models for Differential Problems*. MS&A Series Vol. 16. Springer International Publishing, 2017.
- [39] R. Y. Rubinstein and D. P. Kroese. *Simulation and the Monte Carlo Method*. Wiley, November 2016.
- [40] R. Seydel. *Practical Bifurcation and Stability Analysis*. Interdisciplinary Applied Mathematics. Springer New York, 2009.
- [41] B. W. Silverman. *Density Estimation for Statistics and Data Analysis*. Routledge, 2018.
- [42] R. C. Smith. *Uncertainty Quantification: Theory, Implementation, and Applications*. Society for Industrial and Applied Mathematics, January 2013.
- [43] I. J. Sobey and P. G. Drazin. Bifurcations of two-dimensional channel flows. *Journal of Fluid Mechanics*, 171:263–287, 1986.
- [44] B. Sousedik and H. C. Elman. Stochastic Galerkin methods for the steady-state Navier-Stokes equations. *Journal of Computational Physics*, 316:435–452, 2016.
- [45] N. Sri Namachchivaya. Stochastic bifurcation. *Applied Mathematics and Computation*, 38(2), 1990.
- [46] G. Stefanou. The stochastic finite element method: Past, present and future. *Computer Methods in Applied Mechanics and Engineering*, 198(9–12):1031–1051, February 2009.
- [47] B. Sudret. Global sensitivity analysis using Polynomial Chaos expansions. *Reliability Engineering & System Safety*, 93(7):964–979, July 2008.
- [48] T. J. Sullivan. *Introduction to uncertainty quantification*, volume 63. Springer, 2015.
- [49] N. Tonicello, A. Lario, G. Rozza, and G. Mengaldo. Non-intrusive reduced order models for the accurate prediction of bifurcating phenomena in compressible fluid dynamics. *Computers & Fluids*, 278:106307, 2024.
- [50] D. Venturi, X. Wan, and G. E. Karniadakis. Stochastic bifurcation analysis of Rayleigh–Bénard convection. *Journal of Fluid Mechanics*, 650:391–413, 2010.
- [51] L. Venturi, D. Torlo, F. Ballarin, and G. Rozza. Weighted Reduced Order Methods for Parametrized Partial Differential Equations with Random Inputs. In F. Canavero, editor, *Uncertainty Modeling for Engineering Applications*, pages 27–40. Springer International Publishing, Cham, 2019.
- [52] L. Wang. *Karhunen-Loeve expansions and their applications*. PhD thesis, London School of Economics and Political Science (United Kingdom), 2008.
- [53] D. Xiu. *Numerical Methods for Stochastic computations: a Spectral Method Approach*. Princeton university press, 2010.
- [54] D. Xiu and G. E. Karniadakis. The Wiener-Askey Polynomial Chaos for stochastic differential equations. *SIAM Journal on Scientific Computing*, 24(2):619–644, 2002.
- [55] D. Xiu and G. E. Karniadakis. Modeling uncertainty in flow simulations via generalized Polynomial Chaos. *Journal of Computational Physics*, 187(1):137–167, May 2003.